Cu and Pt clusters deposition on TiO_2 powders by DC magnetron sputtering for photocatalytic hydrogen production

Massimo Bernareggi[a], Gian Luca Chiarello[a,*], Marina Ratova[b], Glen West[b], Anna Maria Ferretti[c], Peter Kelly[b], Elena Selli[a]

[a] *Dipartimento di Chimica, Università degli Studi di Milano, Via Golgi 19, I-20133 Milano, Italy*

[b] *Surface Engineering Group, Manchester Metropolitan University, Manchester, M1 5GD, UK*

[c] *ISTM-CNR Lab Nanotechnology, Via Fantoli 16/15, 20138 Milano, Italy*

A B S T R A C T

Titanium dioxide-based photocatalyst powders were obtained by deposition of copper and/or platinum clusters by means of pulsed direct current magnetron sputtering with different deposition time and plasma composition during Cu sputtering. A top-down configuration was employed with the sputtering source facing the powder holder mounted on a shaker mechanism, which continuously mixed the powders during the sputtering process. HRTEM analyses revealed the presence of well dispersed, subnanometric sized metal clusters, even for long deposition times, while XRD analysis showed no modification of the TiO_2 crystal structure upon metal deposition. The so obtained powders were tested as photocatalysts in methanol photo-steam reforming for hydrogen production. The presence of Pt clusters increased the photoactivity with respect to that of bare TiO_2. The plasma composition during Cu sputtering was found to strongly affect the photoactivity of the obtained materials, Cu alone deposited as co-catalyst in an Ar-only atmosphere imparting better photoactivity than Cu sputtered in Ar/O_2. When the deposition of Cu clusters was coupled with the deposition of Pt clusters, an additive effect of the two metals in increasing TiO_2 photoactivity was observed only if Cu clusters were sputtered in the absence of oxygen.

* Corresponding author. Tel: +39 02 503 14281; fax: +39 02 503 14300.
E-mail address: gianluca.chiarello@unimi.it

1. Introduction

Hydrogen is often considered the fuel for the future due to its pollution-free nature [1]. However, H_2 production is still a major problem being far from being environmentally friendly. In this context, photocatalytic steam reforming, conceivably exploiting biomass as organic hole scavenger, could be a viable alternative to traditional H_2 production processes [2]. Titanium dioxide, despite its relatively large bandgap [4], is still one of the most effective photocatalyst, due to its photostability and peculiar physico-chemical properties [3]. The photocatalytic performance can be increased in the presence of an organic compound, such as methanol, ethanol or glycerol, acting as hole scavenger [5–7], and of noble metal (Au, Pt, Pd, Ag) nanoparticles on the semiconductor surface acting as efficient electron traps [5,8]. Further addition of non-noble metal (*i.e.* Cu or Ni) nanoparticles may increase the photocatalytic activity and also lead to visible light activation of the photocatalysts [9–11]. Among all, titanium dioxide-based materials modified with both a noble metal and a non-noble metal, *e.g.* with Pt and Cu, respectively, proved to be more efficient than the corresponding monometallic materials. Recently, some of us reported high photocatalytic hydrogen productions with Cu and Pt nanoparticle-containing TiO_2 photocatalysts obtained either by Cu grafting followed by Pt deposition [12] or by flame spray pyrolysis in a single step [13].

Pulsed-Direct Current (p-DC) magnetron sputtering (MS) is a well-known technique used for the production of thin films. This technology is widely employed also on the industrial scale due to its scalability and versatility, and to the repeatability and high quality of the obtained coatings. In fact, MS is exploited for many applications, ranging from solar glazing products to micro-electronic coatings, from tool protecting layers to packaging coatings [14], allowing the deposition of both metallic and non-metallic coatings over various substrates. Recently, p-DC MS has been employed on the laboratory scale also for metal nanoparticles production and deposition on the surface of solid [15–18] or liquid supports [19–21], thus avoiding the contaminations of solvents and/or precursors typically occurring with more conventional techniques.

So far, the possibility of exploiting this technique to modify materials in powder form has been investigated only by the group of Teixeira *et al.* [16,17], who found that high metal loadings (larger than 0.5 wt.%) can be obtained even with short sputtering times. The great enhancement of the catalytic activity of the so obtained materials was attributed to the unimodal distribution and small average diameters (*ca.* 1.5 nm) of the deposited metal nanoparticles.

In this work, we present our preliminary results on Cu and/or Pt clusters deposition on TiO_2 powders by p-DC-MS, employing a home-made apparatus [22]. This set-up is based on an oscillating bowl (powder holder) placed under the magnetrons. The oscillations force the powder particles to roll and mix around the bowl while the metal atoms are evaporated from the magnetron target. The obtained materials were tested as photocatalysts in the methanol photo-steam reforming reaction for hydrogen production, according to the reaction: $CH_3OH + H_2O \xrightarrow{h\nu} 3\ H_2 + CO_2$.

2. Experimental

2.1. Photocatalytic materials

Copper and platinum were deposited over commercial P25 TiO_2 powders (Sigma-Aldrich) by pulsed direct current (p-DC) magnetron sputtering (MS) in the already described rig [23]. A sketch of the employed set-up is shown in Fig. 1. Briefly, the deposition system consisted in a sputter-down configuration, with a single 7.5 cm diameter type II unbalanced planar magnetron installed on the roof of the sputtering chamber. Thus, the target was facing an electrically floating substrate holder placed 5 cm underneath the magnetron, allowing a continuous powder mixing during the sputtering process via a shaker mechanism. The magnetron was powered by an Advanced Energy Pinnacle Plus power supply. The metal targets were sputtered at 250 W, 350 kHz, 50% duty cycle (corresponding to a pulse-off period of 1.4 μs, when the cathode voltage is reversed). The deposition process was performed in an Ar-only atmosphere for both Pt and Cu deposition and also in a 1:1 O_2/Ar plasma for copper deposition. The working pressure was fixed, for all depositions, at *ca.* 2.6 Pa, after having evacuated the chamber below $5 \cdot 10^{-3}$ Pa by means of a rotary (Leybold

Ttrivac 16B) and a turbomolecular (Leybold TurboVac i90) pump. The desired pressure was achieved by adjusting the gate valve between the chamber and the turbomolecular pump. The total gas flow during deposition was fixed at 20 sccm for all runs.

3 g of P25 TiO_2 were treated for different time (1-10 min) in different atmospheres. The so obtained modified photocatalyst samples are named as "P25" followed by deposition time (in min) and by the symbol of the sputtered metal(s), in the order in which they were deposited. In the case of copper, the Cu symbol is also followed by the main gas used during deposition. For instance, P25+1Cu-O_2+5Pt indicates the P25-based sample first modified by a 1-min long Cu deposition in O_2/Ar atmosphere followed by a 5 min-long platinum deposition in argon. Copper deposition always preceded platinum deposition, as in previous work [12] in which the two metals were deposited by different techniques.

2.2. Photocatalyst characterisation

UV-vis diffuse reflectance spectra of all powders were recorded on a Jasco V-670 spectrophotometer equipped with a PIN-757 integrating sphere using barium sulphate as a reference. The reflectance R was then converted in absorption according to: $A = 1 - R$.

X-Ray powder diffraction (XRPD) was carried out with a Panalytical Xpert diffractometer operating at 40 kV voltage and 30 mA current using the Cu Kα radiation (λ = 1.54056 Å), with the patterns recorded in the $20° < 2\theta < 100°$ range (scan step = 0.013°). The crystal phase composition was evaluated by Rietveld refinement [24] using the Quanto software [25]. The Scherrer equation, from the most intense reflection at 2θ = 25.4°, was exploited to calculate the mean anatase crystallite size [26].

Inductively Coupled Plasma Optical Emission Spectroscopy (ICP-OES) analyses were performed with a Perkin Elmer Optima 8000 ICP-OES. Pt and Cu were dissolved by dispersing the sample in aqua regia (3:1 HCl:HNO_3 solution) at 90 °C for 3 hours.

HRTEM analysis was carried out with a Zeiss LIBRA 200FE transmission electron microscope, equipped with STEM—HAADF and EDX (Oxford X-Stream 2 and INCA software). The microscope has a 200 kV field emission gun-like source with an in-column second-generation Omega filter for energy-selective spectroscopy. The samples were dispersed in isopropanol and then a drop of the suspension was deposited on a 300 mesh holey carbon copper (for Pt containing samples) or molybdenum (for Cu containing samples) grid.

2.3. Photocatalytic tests

The photocatalysts were tested in hydrogen production from methanol photo-steam reforming reaction by exploiting the recirculating stainless-steel closed system described elsewhere [13]. (15±2) mg of sample were dispersed in *ca.* 1 mL of MilliQ water and mixed with (7.10±0.05) g of quartz grains (20–40 mesh) and then dried in oven at 70 °C for at least 2 h. The so-obtained photocatalytic bed was loaded into the home-made steel photoreactor, closed with a Pyrex glass window. Before starting any run, the system was thoroughly purged with pure nitrogen in order to remove any trace of oxygen from both the gas phase and the 20 vol% methanol/water solution, kept at 30 °C. The gas phase, saturated with the solution vapours, was recirculated by means of a metal Bellows pump at 60 mL min^{-1}. The photocatalytic bed was irradiated by a 300W Xenon arc lamp (LOT-Oriel), switched on 30 min before the run and positioned at 20 cm from the photoreactor, providing an incident power of *ca.* 120 mW cm^{-2} on the photocatalyst, as measured with a calibrated Thorlabs S130VC photodiode.

The recirculating phase was sampled and analysed automatically at regular intervals by a gas-chromatograph (Agilent 6890N) equipped with two columns (Molesieve 5A and HP-PlotU), two detectors (flame ionisation and thermo conductivity) and a Ni-catalyst system for CO and CO_2 methanation. Formic acid production was evaluated by analysing the liquid solution with an ion chromatograph (Metrohm 761 Compact IC) at the end of any run.

The photocatalytic tests were repeated at least twice in order to ensure the reproducibility of data. At the end of each run, the liquid solution was replaced with a new one and the system was thoroughly purged in pure nitrogen in the dark for 40 min before starting a new run.

3. Results and discussion

3.1. Photocatalysts characterisation

The results of elemental ICP analysis on the produced photocatalysts are collected in Table 1. The platinum loading is *ca.* twice the copper loading attained under analogous sputtering conditions, with *ca.* 0.7 wt.% Pt *vs. ca.* 0.34 wt.% Cu deposited after 10 min-long deposition. This is actually due to the much higher atomic weight of Pt with respect to Cu (195 *vs.* 63.5, respectively). Indeed, the average deposition rate of Cu under Ar atmosphere is significantly higher than that of Pt (*e.g.*, 8.9 *vs.* 6.1 μmol s^{-1} after 10 min-long deposition, respectively). This is consistent with the higher relative sputtering yield of Cu with respect to that of Pt. The average deposition rate of Pt increased with increasing overall deposition time, while that of Cu decreased. As expected, the presence of O_2 during the sputtering process caused an important decrease in the Cu sputtering yield since after 10 min deposition only 0.1 wt.% Cu was deposited on the TiO_2 powder under such conditions.

The absorption spectra of the prepared materials shown in Fig. 2 confirm that Cu and/or Pt clusters were deposited on the TiO_2 surface, because a characteristic absorption appeared in the visible region. No shift in the band gap absorption onset could be observed in the spectra of the modified samples compared to that of pristine TiO_2. Thus, the room temperature sputtering process in vacuum does not affect the main structural characteristics of the supporting powder, in contrast with other metal deposition methods, *e.g.* grafting or deposition-precipitation [12], which imply a post-thermal treatment of the material.

Pt-modified TiO_2 materials show an extended absorption in the visible range due to the presence of the noble metal that makes these samples greyish (Fig. 2a). As expected, the absorption in the 400-800 nm range increases for longer deposition times, in agreement with the Pt loading increase.

The absorption spectra of Cu modified TiO_2 materials are characterized by the presence of a typical absorption band in the 600–800 nm region, due to the Cu *d-d* transition, and/or an absorption tail in the 400–500 nm region attributed to the interfacial charge transfer (IFCT) phenomenon between TiO_2 valence band electrons and Cu(II) species [12]. The absorption spectra of the photocatalysts modified with Cu sputtering in an Ar-only atmosphere (see Fig. 2b) exhibit an absorption in the visible range, due to the presence of copper nanoparticles, increasing with increasing deposition time, but no absorption tail between 400 and 500 nm related to an IFCT. Such absorption feature appears only in the absorption spectrum of P25+1Cu-O_2 (Fig. 2c), suggesting the presence of atomically dispersed Cu(II) species (consistent with its unique yellowish colour) in the low copper loading deposited in an oxidising atmosphere. Moreover, the absorption spectra of the photocatalysts obtained by Cu sputtering in an Ar/O_2 plasma (Fig. 2c) show a weaker absorption in the visible range with respect to the absorption spectra of the analogous photocatalysts obtained by Cu sputtering in an Ar-only atmosphere. This is compatible with the lower deposition rate attained under reactive conditions. Finally, the absorption spectra of the Cu and Pt co-modified samples are basically dominated by the absorption profile of Pt nanoparticles in the visible region.

Fig. 3 shows that the XRPD patterns of the metal modified materials are identical to that of pristine TiO_2. In fact, the Rietveld refinement of XRPD data confirmed that the amount of anatase and rutile phases did not change after metal deposition, as well as the anatase crystallite mean size, calculated through the Scherrer equation (see Table 2). All samples are composed of a mixture of *ca.* 85% anatase and 15% rutile, with an average anatase crystalline size of 23 nm. No additional reflections related to metal Pt and Cu or copper oxides can be observed, due to their low loading and fine dispersion on the TiO_2 surface.

The STEM—HAADF and EDX analyses of P25+10Pt shown in Fig. 4 reveal that the Pt particles are irregularly dispersed on the TiO_2 surface. In particular, areas with finely dispersed Pt clusters (area 1 in Fig. 4 and its magnification shown in Fig. 5b) can be distinguished from areas with dense aggregates of Pt nanoparticles (area 2 in Fig. 4 and its magnification shown in Fig. 5a). This is very likely due to a non-perfect mixing of the powder during the sputtering process and generates a bimodal distribution of the Pt particles size, as shown in Fig. 5d. In particular, the mean particle size obtained by fitting the distribution with two Gaussian functions are 0.8 nm (0.5 nm standard deviation) and 2.2 nm (1.1 nm standard deviation). This particle size is similar or even smaller than that recently attained with other techniques, such as deposition-precipitation or flame spray pyrolysis [27], or even pDC-MS [16].The EDX quantitative elemental analysis of Pt in Area 1 of Fig. 4 gives a 0.7 wt.% Pt loading, while that of area 2 yields a 18 wt.% Pt loading. The Pt loading of area 1 measured by EDX is in agreement with the overall Pt loading determined by ICP analysis (0.71 wt.%, see Table 1). Thus, we can tentatively conclude that the major fraction of Pt is present in the form of well dispersed clusters (*i.e.* with particles size below 2 nm) together with some islands of Pt nanoparticle aggregates (it must be taken into account that HRTEM is a local probe). Similar Pt particles shape and distribution was detected by HRTEM analysis independently of the deposition time (*i.e.* in samples with different metal loadings). This suggests that different deposition settings, for instance a lower sputtering power (*i.e.,* a lower Pt evaporation rate), as well as longer deposition time could lead to a more uniform Pt clusters distribution.

Fig. 5c shows the HRTEM image of P25+10Cu-Ar. Cu clusters are more difficult to detect by STEM than Pt clusters, because Cu has a Z-contrast similar to that of Ti. Nevertheless, some Cu clusters can be recognized on the TiO_2 surface, with a shape and dispersion similar to those of Pt clusters.

3.2. Methanol photo-steam reforming tests

During the photocatalytic steam reforming process, methanol undergoes oxidation up CO_2 through the formation of formaldehyde and formic acid as intermediates, while methane, CO, and dimethylether are usually found as main side products, as already reported in previous work [27]. The gaseous products (H_2, CO_2 and CO) accumulate at constant rate in the recirculating gas phase within the same run (pseudo zero-order kinetics).

As expected, the presence of Pt clusters on the TiO_2 surface is beneficial to the photoactivity of the material, regardless of their amount. Indeed, the work-function of Pt (5.12 − 5.93 eV) is larger than that of TiO_2 (4.6 – 4.7 eV) and a larger work function implies a Fermi level located at lower energy. Thus, the electrons photopromoted into the TiO_2 conduction band are easily transferred to Pt clusters, while photoproduced holes remain in the TiO_2 valence band, with the consequent decrease of electron-hole pair recombination probability. The work function of Cu is 4.53 − 5.10 eV, *i.e.* lower than that of Pt but in a range that can exceed that of TiO_2. This implies that also metallic Cu can in principle act as sink of photopromoted electrons, though being less efficient than Pt. In fact, the highest photocatalytic performance was attained with P25+10Pt, the photocatalyst obtained by 10 min-long Pt sputtering, leading to a 6-fold increase in H_2 production rate (r_{H_2}) with respect to that of bare titania (Fig. 6a). The selectivity towards CO and H_2CO decreases with increasing Pt amount in the photocatalyst, while the opposite occurs for CO_2 and HCOOH (Table 3). These effects are well established for Pt-modified TiO_2 because the noble metal is very effective in pushing methanol oxidation up to CO_2.

A similar behaviour, but to a lesser extent, can be observed for photocatalysts modified with Cu clusters sputtered in Ar-only plasma (Fig. 6b). For photocatalysts containing one of the two sputtered metals, r_{H_2} increased with increasing metal loading. In the case of P25+10Cu-Ar, a 4-fold increase of r_{H_2} was achieved with respect to that of bare titania. Conversely, Cu deposition in a reactive environment (*i.e.* O_2/Ar plasma) was detrimental in the case of P25+1Cu-O_2, or gave very low photoactivity enhancement (Fig. 6c), P25+10Cu-O_2 being the only photocatalyst of this series

showing an increased H_2 production rate with respect to bare TiO_2. Thus, for this type of reaction copper in reduced state appears to be a more performing co-catalyst of TiO_2 than copper oxides [28].

By comparing the two Cu-only modified photocatalyst series, sputtering copper in Ar-only gives better results than sputtering copper in $Ar+O_2$ atmosphere. This is possibly related to the lower Cu loading achieved after the same deposition time, due to the lower copper evaporation rate in O_2 containing plasma, and also to the different Cu oxidation state. In particular, the photocatalytic performance attained with P25+1Cu-O_2 is lower than that of pristine TiO_2 (Fig. 6c). P25+1Cu-O_2 is the only sample showing the characteristic IFCT absorption feature in Fig. 2c, involving the direct transition of an electron from the TiO_2 valence band to surface Cu(II) species with the consequent copper reduction to Cu(I). However, the redox potential of C(II)/Cu(I) couple is expected to be more positive than that of the H^+/H_2 couple. Thus, electrons photopromoted into the copper oxide clusters are not useful for hydrogen production and Cu(I) can be oxidized back to Cu(II) by valence band holes with the consequent loss of photon energy and decrease of the overall photocatalytic performance.

TiO_2 was also modified by deposition of both metals, Cu sputtering always preceding Pt sputtering, in line with the deposition sequence optimised in previous studies [12]. The Pt deposition time was fixed at 5 min, while Cu was sputtered for either 1 or 5 min. Fig. 6d shows that with the photocatalysts obtained by sputtering copper in an Ar-only plasma for 1 or 5 min the rate of hydrogen production (9.6 mmol h^{-1} g_{cat}^{-1}) was close to the sum of the rates attained with the corresponding single-metal modified materials. Thus, in such materials copper and platinum clusters on the TiO_2 surface appear to have additive, rather than synergistic effects on photoactivity. A similar r_{H2} value was also attained with P25+1Cu-O_2+5Pt, while the corresponding Cu-only modified P25+1Cu-O_2 sample showed very low photoactivity. Thus, in this case the hydrogen production rate value was larger than the sum of the H_2 production rates obtained with the singly modified materials, possibly due to almost complete copper reduction during Pt sputtering. This

behaviour is similar to that reported in a recent work of some of us [12]. In contrast, larger amounts of copper sputtered in the presence of O_2, followed by Pt sputtering, proved to have negative effects on the photocatalytic activity, with a decrease of r_{H2} down to 6.3 mmol h^{-1} g_{cat}^{-1} in the case of P25+1Cu-O_2+5Pt. Moreover, Fig. 6d shows that all Pt-Cu co-modified materials, apart from P25+1Cu-O_2+5Pt, showed very similar hydrogen production rates, suggesting that the presence of Pt clusters on the TiO_2 surface is determining their photoactivity.

4. Conclusions

This work demonstrates that pulsed-DC magnetron sputtering is a potential excellent technique to produce large amounts of photocatalyst powders modified with tailored metal nanoparticles in short time, also avoiding any structural change of the starting material. The operation conditions need to be optimized to increase the homogeneity of the metal clusters dispersion, for instance, by lowering the sputtering power and by adopting longer deposition times, or a higher shaking frequency during metal sputtering. The properties of the deposited metal clusters also depend on the composition of the plasma during metal sputtering. In fact, when sputtered under Ar-only plasma, Cu sputtered clusters on TiO_2 behave as typical metal co-catalysts, enhancing TiO_2 photoactivity with increasing loading, but without any synergistic effect when co-deposited with Pt.

Tables

Table 1. ICP results reporting Pt and/or Cu loading on different samples and average metal deposition rate calculated by the wt.% divided by the overall deposition time.

Sample	Dep. time (s)	Amount (wt.%)		Average dep. rate (μmol s^{-1})	
		Pt	Cu	Pt	Cu
P25+1Pt	60	0.04	/	3.4	
P25+10Pt	600	0.71	/	6.1	
P25+1Cu-Ar+5Pt	60 + 300	0.19	0.07	3.2	18.4
P25+1Cu-Ar	60	/	0.05		13.1
P25+10Cu-Ar	600	/	0.34		8.9
P25+10Cu-O_2	600	/	0.09		2.4

Table 2. Average diameter of anatase nanoparticles and crystal phase composition.

Sample	$d_{anatase}$ (nm)	Anatase (%)	Rutile (%)
P25	23.5	85.8	14.2
P25+10Pt	23.0	84.9	15.1
P25+10Cu-Ar	23.4	86.4	13.6
P25+10Cu-O_2	23.7	86.8	13.2

Table 3. Photocatalytic performance of the investigated materials in methanol photo-steam reforming, in terms of rates of products formation, *r*, and percent selectivity in relation to hydrogen production, *S*. Reaction conditions: 0.015 g of photocatalyst fed in recirculation mode with 60 mL min^{-1} of a 2% CH_3OH / 3% H_2O / N_2 (balance) gas mixture

	Production rate / mmol h^{-1} g_{cat}^{-1}						Selectivity in relation to H_2 production / %			
Photocatalyst	H_2	CO_2	CO	H_2CO	HCO_2H	CH_4	CO_2	CO	H_2CO	HCO_2H
P25	1.63	0.10	0.12	1.76	0.17	$8 \cdot 10^{-4}$	18.8	15.7	67.2	21.3
P25+1Pt	3.32	0.22	0.22	2.33	0.33	$2 \cdot 10^{-3}$	19.8	13.0	39.2	19.7
P25+5Pt	7.73	0.81	0.38	3.74	0.73	$3 \cdot 10^{-3}$	31.4	9.8	27.1	18.9
P25+10Pt	10.03	1.12	0.36	4.93	1.40	$6 \cdot 10^{-3}$	33.4	7.2	25.9	28.0
P25+1Cu-Ar	1.80	0.11	0.13	1.63	0.24	$7 \cdot 10^{-4}$	18.5	14.6	51.0	26.4
P25+5Cu-Ar	3.20	0.33	0.21	2.58	0.35	$7 \cdot 10^{-4}$	25.8	15.2	63.4	22.1
P25+10Cu-Ar	3.68	0.93	0.34	3.29	0.88	$2 \cdot 10^{-3}$	42.0	10.0	27.6	26.5
P25+1Cu-O_2	0.59	0.03	0.05	1.13	0.07	$8 \cdot 10^{-4}$	14.8	17.3	116.1	25.6
P25+5Cu- O_2	1.62	0.10	0.12	1.20	0.19	$5 \cdot 10^{-4}$	18.6	14.6	41.3	23.8
P25+10Cu- O_2	2.75	0.21	0.17	1.84	0.34	$2 \cdot 10^{-3}$	22.9	12.4	37.7	24.8
P25+1Cu-Ar+5Pt	9.63	1.18	0.42	4.21	0.85	$3 \cdot 10^{-3}$	36.8	8.7	24.5	17.5
P25+5Cu-Ar+5Pt	9.67	1.42	0.40	3.55	1.01	$4 \cdot 10^{-3}$	44.1	8.3	20.6	20.8
P25+1Cu-O_2+5Pt	9.62	1.10	0.39	4.51	1.01	$2 \cdot 10^{-3}$	34.4	8.2	26.3	21.0
P25+5Cu- O_2+5Pt	6.31	0.61	0.30	3.99	0.56	$1 \cdot 10^{-3}$	28.8	9.6	35.4	17.7

Figure captions

Figure 1. Sketch of the employed p-DC magnetron sputtering set up.

Figure 2. Absorption spectra of the a) P25+xPt, b) P25+xCu-Ar, c) P25+xCu-O_2, (x = 1, 5 and 10 min); d) Cu and Pt co-modified photocatalyst series, all compared the absorption spectrum of bare P25 TiO_2 (dashed black line).

Figure 3. XRPD patterns of selected samples. The inset shows superimposed patterns in the 2θ 24–28° range, demonstrating that the sputtering treatment did not alter the crystal structure.

Figure 4. STEM—HAADF + EDX analysis of the P25+10Pt sample.

Figure 5. (a) STEM-HAADF image of P25+10Pt and HRTEM micrographs of (b) P25+10Pt and (c) P25+10Cu-Ar. (d) Pt particle size distribution of P25+10Pt. The red curve is the distribution fitting obtained using two Gaussian curves (green curves). The red arrows in (b) and (c) point to Pt and Cu clusters, respectively.

Figure 6. Hydrogen and by-products production rates obtained with (a) Pt-modified TiO_2, (b) Ar-sputtered Cu-modified TiO_2, (c) Ar/O_2-sputtered Cu-modified TiO_2, (d) Pt and Cu co-modified TiO_2, compared to bare, unmodified P25 TiO_2.

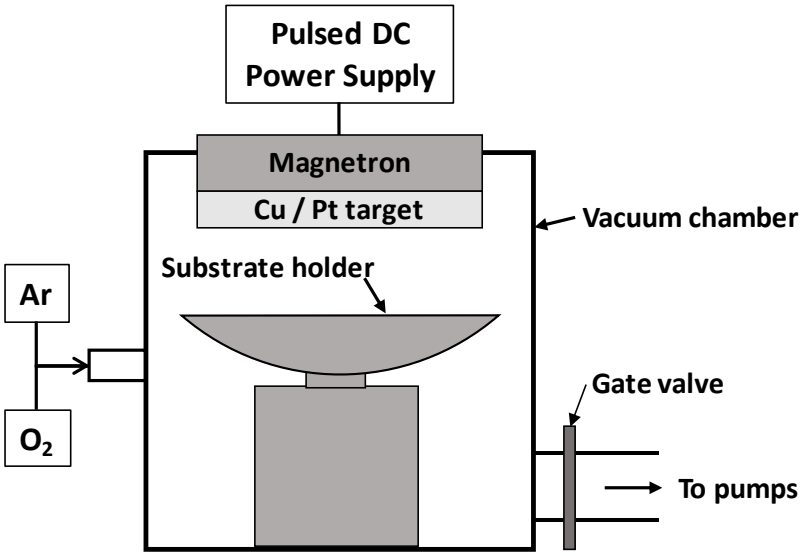

Figure 1. Sketch of the employed p-DC magnetron sputtering set up.

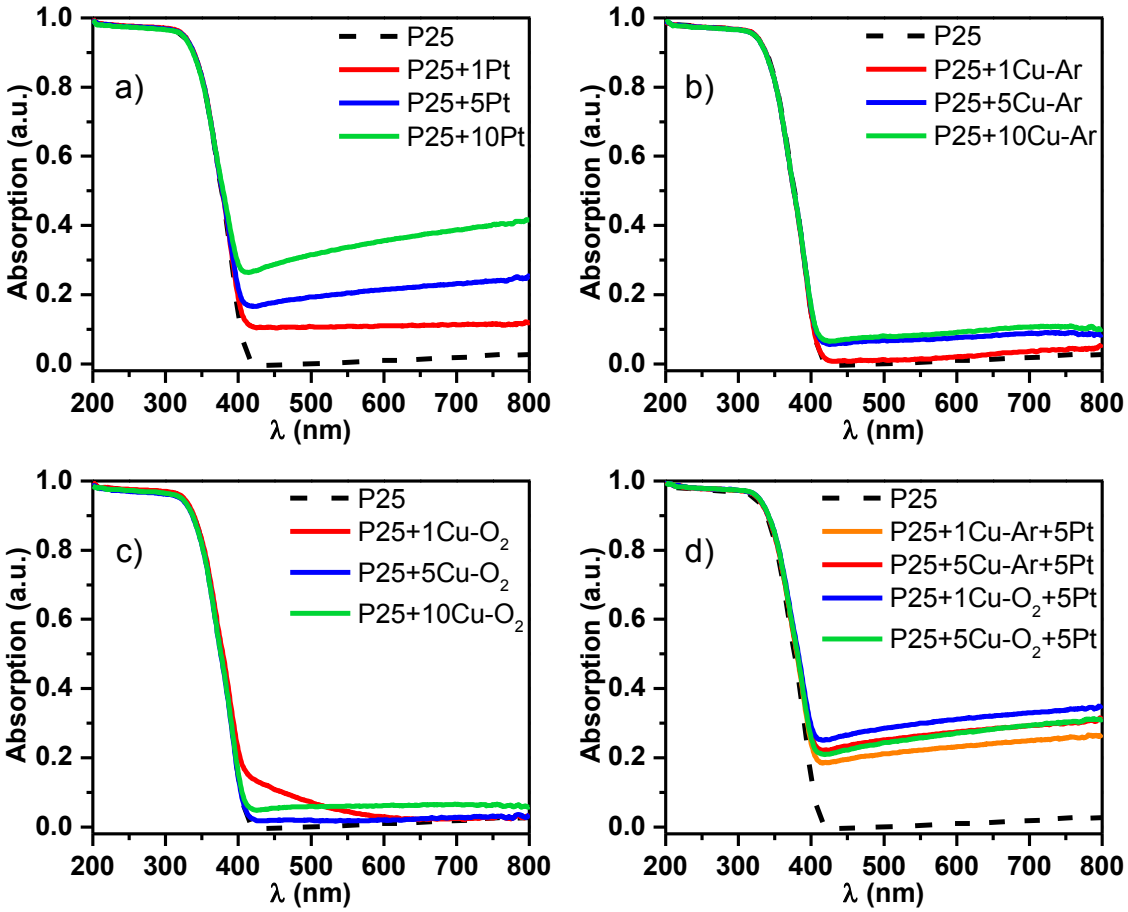

Figure 2. Absorption spectra of the (a) P25+XPt, (b) P25+XCu-Ar, (c) P25+XCu-O_2, (d) Cu and Pt co-modified photocatalyst series, all compared the absorption spectrum of bare P25 TiO_2 (dashed black line). X = 1, 5, 10 min

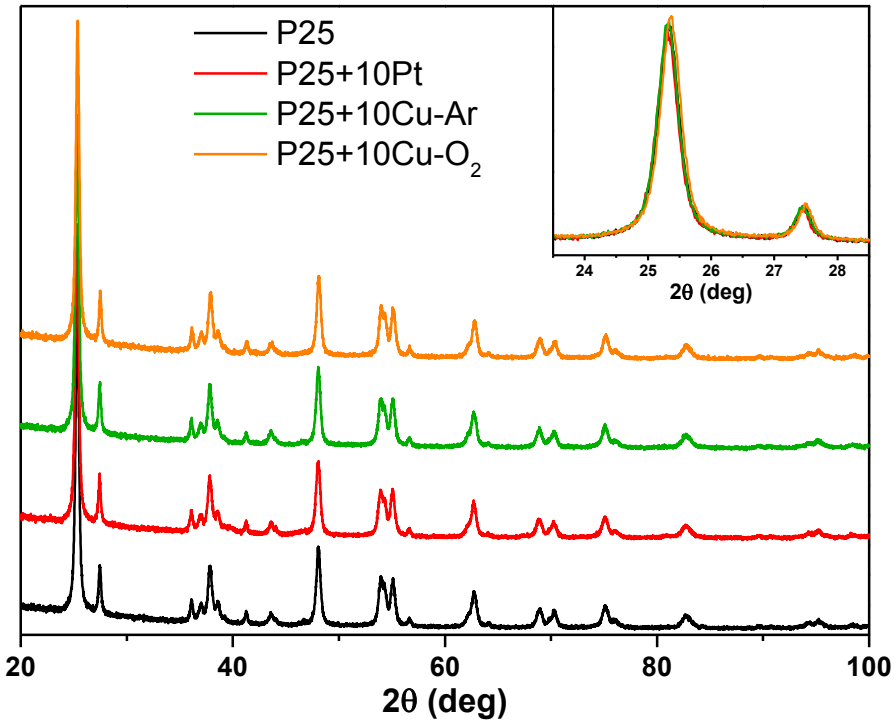

Figure 3. XRPD patterns of selected samples. The inset shows superimposed patterns in the 2θ 24–28° range, demonstrating that the sputtering treatment did not alter the crystal structure.

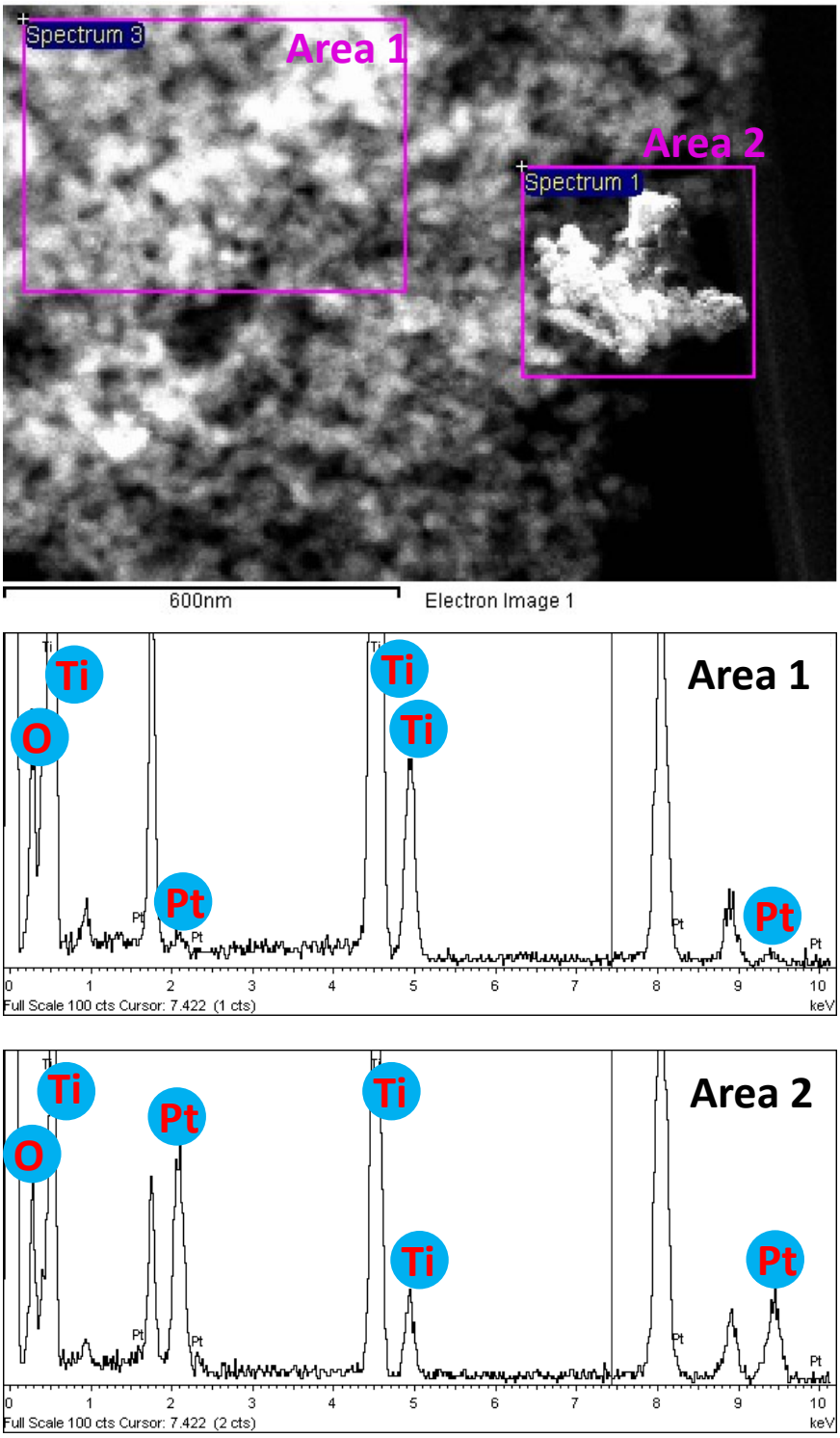

Figure 4. STEM—HAADF + EDX analysis of the P25+10Pt sample.

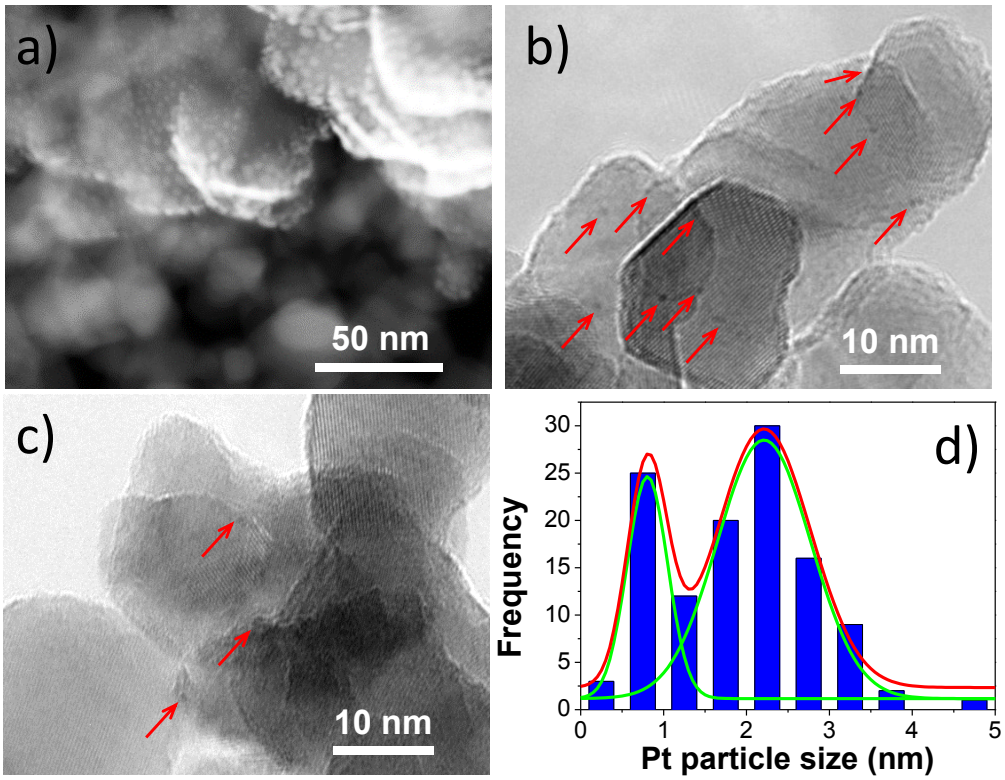

Figure 5. (a) STEM-HAADF image of P25+10Pt and HRTEM micrographs of (b) P25+10Pt and (c) P25+10Cu-Ar. (d) Pt particle size distribution of P25+10Pt. The red curve is the distribution fitting obtained using two Gaussian curves (green curves). The red arrows in (b) and (c) point to Pt and Cu clusters, respectively.

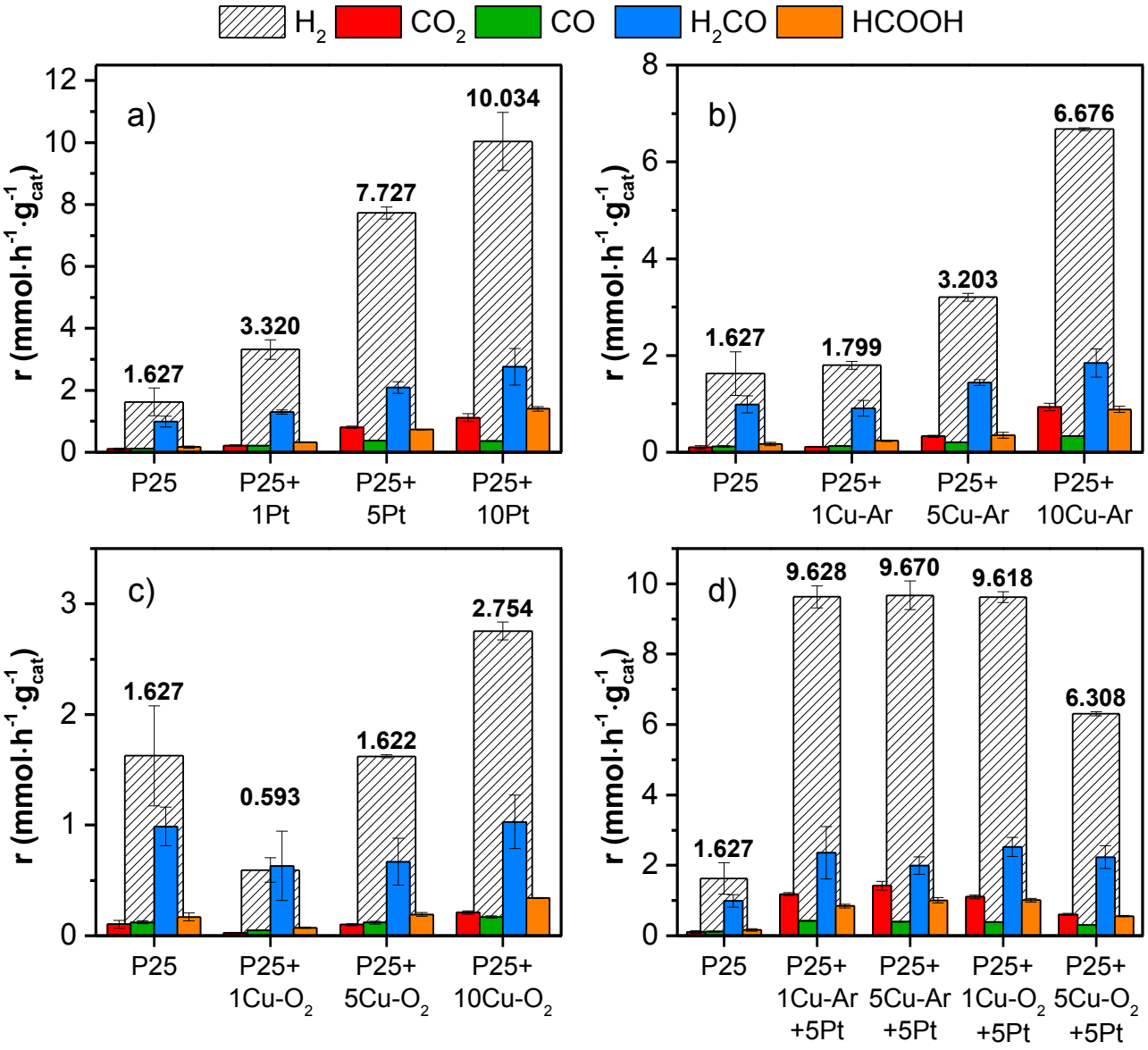

Figure 6. Hydrogen and by-products production rates obtained with (a) Pt-modified TiO_2, (b) Ar-sputtered Cu-modified TiO_2, (c) Ar/O_2-sputtered Cu-modified TiO_2, (d) Pt and Cu co-modified TiO_2, compared to bare, unmodified P25 TiO_2.

References

[1] K. Rajeshwar, R. McConnel, S. Licht, Solar Hydrogen Generation, Springer New York, New York, NY, 2008. doi:10.1007/978-0-387-72810-0.

[2] A. V. Puga, Photocatalytic production of hydrogen from biomass-derived feedstocks, Coord. Chem. Rev. 315 (2016) 1–66. doi:10.1016/j.ccr.2015.12.009.

[3] Y. Ma, X.L. Wang, Y.S. Jia, X.B. Chen, H.X. Han, C. Li, Titanium Dioxide-Based Nanomaterials for Photocatalytic Fuel Generations, Chem. Rev. 114 (2014) 9987–10043. doi:10.1021/cr500008u.

[4] J. Schneider, M. Matsuoka, M. Takeuchi, J. Zhang, Y. Horiuchi, M. Anpo, D.W. Bahnemann, Understanding TiO_2 Photocatalysis: Mechanisms and Materials, Chem. Rev. 114 (2014) 9919–9986. doi:10.1021/cr5001892.

[5] G.L. Chiarello, M.V. Dozzi, E. Selli, TiO_2 -based materials for photocatalytic hydrogen production, J. Energy Chem. 26 (2017) 250–258. doi:10.1016/j.jechem.2017.02.005.

[6] H.J. Choi, M. Kang, Hydrogen production from methanol/water decomposition in a liquid photosystem using the anatase structure of Cu loaded TiO_2, Int. J. Hydrogen Energy. 32 (2007) 3841–3848. doi:10.1016/j.ijhydene.2007.05.011.

[7] T. Kawai, T. Sakata, Conversion of carbohydrate into hydrogen fuel by a photocatalytic process, Nature. 286 (1980) 474–476. doi:10.1038/286474a0.

[8] G.L. Chiarello, E. Selli, Photocatalytic Hydrogen Production, Recent Patents Eng. 4 (2010) 155–169. doi:10.2174/187221210794578600.

[9] M.G. Méndez-Medrano, E. Kowalska, A. Lehoux, A. Herissan, B. Ohtani, D. Bahena, V. Briois, C. Colbeau-Justin, J.L. Rodríguez-López, H. Remita, Surface Modification of TiO_2 with Ag Nanoparticles and CuO Nanoclusters for Application in Photocatalysis, J. Phys. Chem. C. 120 (2016) 5143–5154. doi:10.1021/acs.jpcc.5b10703.

[10] A.L. Luna, E. Novoseltceva, E. Louarn, P. Beaunier, E. Kowalska, B. Ohtani, M.A. Valenzuela, H. Remita, C. Colbeau-Justin, Synergetic effect of Ni and Au nanoparticles synthesized on titania particles for efficient photocatalytic hydrogen production, Appl. Catal. B Environ. 191 (2016) 18–28. doi:10.1016/j.apcatb.2016.03.008.

[11] M. Nischk, P. Mazierski, Z. Wei, K. Siuzdak, N.A. Kouame, E. Kowalska, H. Remita, A. Zaleska-Medynska, Enhanced photocatalytic, electrochemical and photoelectrochemical properties of TiO_2 nanotubes arrays modified with Cu, AgCu and Bi nanoparticles obtained via radiolytic reduction, Appl. Surf. Sci. 387 (2016) 89–102. doi:10.1016/j.apsusc.2016.06.066.

[12] M.V. Dozzi, G.L. Chiarello, M. Pedroni, S. Livraghi, E. Giamello, E. Selli, High Photocatalytic Hydrogen Production on Cu(II) Pre-grafted Pt/TiO_2, Appl. Catal. B Environ. 209 (2017) 417–428. doi:10.1016/j.apcatb.2017.03.007.

[13] M. Bernareggi, M.V. Dozzi, L. Bettini, A. Ferretti, G.L. Chiarello, E. Selli, Flame-Made Cu/TiO_2 and Cu-Pt/TiO_2 Photocatalysts for Hydrogen Production, Catalysts. 7 (2017) 301. doi:10.3390/catal7100301.

[14] P.J. Kelly, R.. Arnell, Magnetron sputtering: a review of recent developments and applications, Vacuum. 56 (2000) 159–172. doi:10.1016/S0042-207X(99)00189-X.

[15] Y. Zhang, H. Ma, M. Yi, Z. Shen, X. Yu, X. Zhang, Magnetron-sputtering fabrication of noble metal nanodots coated TiO_2 nanoparticles with enhanced photocatalytic performance, Mater. Des. 125 (2017) 94–99. doi:10.1016/j.matdes.2017.03.084.

[16] M.P. Languer, F.R. Scheffer, A.F. Feil, D.L. Baptista, P. Migowski, G.J. Machado, D.P. De Moraes, J. Dupont, S.R. Teixeira, D.E. Weibel, Photo-induced reforming of alcohols with improved hydrogen apparent quantum yield on TiO_2 nanotubes loaded with ultra-small Pt nanoparticles, Int. J. Hydrogen Energy. 38 (2013) 14440–14450. doi:10.1016/j.ijhydene.2013.09.018.

[17] R. V. Gonçalves, R. Wojcieszak, H. Wender, C. Sato B. Dias, L.L.R. Vono, D. Eberhardt,

S.R. Teixeira, L.M. Rossi, Easy Access to Metallic Copper Nanoparticles with High Activity and Stability for CO Oxidation, ACS Appl. Mater. Interfaces. 7 (2015) 7987–7994. doi:10.1021/acsami.5b00129.

[18] R. V. Gonçalves, R. Wojcieszak, P.M. Uberman, D. Eberhardt, E. Teixeira-Neto, S.R. Teixeira, L.M. Rossi, Catalytic abatement of CO over highly stable Pt supported on Ta_2O_5 nanotubes, Catal. Commun. 48 (2014) 50–54. doi:10.1016/j.catcom.2014.01.020.

[19] H. Wender, P. Migowski, A.F. Feil, L.F. de Oliveira, M.H.G. Prechtl, R. Leal, G. Machado, S.R. Teixeira, J. Dupont, On the formation of anisotropic gold nanoparticles by sputtering onto a nitrile functionalised ionic liquid, Phys. Chem. Chem. Phys. 13 (2011) 13552. doi:10.1039/c1cp21406c.

[20] H. Wender, R. V. Gonçalves, A.F. Feil, P. Migowski, F.S. Poletto, A.R. Pohlmann, J. Dupont, S.R. Teixeira, Sputtering onto Liquids: From Thin Films to Nanoparticles, J. Phys. Chem. C. 115 (2011) 16362–16367. doi:10.1021/jp205390d.

[21] H. Wender, P. Migowski, A.F. Feil, S.R. Teixeira, J. Dupont, Sputtering deposition of nanoparticles onto liquid substrates: Recent advances and future trends, Coord. Chem. Rev. 257 (2013) 2468–2483. doi:10.1016/j.ccr.2013.01.013.

[22] M. Ratova, P.J. Kelly, G.T. West, L. Tosheva, M. Edge, Reactive magnetron sputtering deposition of bismuth tungstate onto titania nanoparticles for enhancing visible light photocatalytic activity, Appl. Surf. Sci. 392 (2017) 590–597. doi:10.1016/j.apsusc.2016.09.035.

[23] M. Ratova, R. Klaysri, P. Praserthdam, P.J. Kelly, Pulsed DC magnetron sputtering deposition of crystalline photocatalytic titania coatings at elevated process pressures, Mater. Sci. Semicond. Process. 71 (2017) 188–196. doi:10.1016/j.mssp.2017.07.028.

[24] H.M. Rietveld, A profile refinement method for nuclear and magnetic structures, J. Appl. Crystallogr. 2 (1969) 65–71. doi:10.1107/S0021889869006558.

[25] A. Altomare, M.C. Burla, C. Giacovazzo, A. Guagliardi, A.G.G. Moliterni, G. Polidori, R. Rizzi, Quanto : a Rietveld program for quantitative phase analysis of polycrystalline mixtures, J. Appl. Crystallogr. 34 (2001) 392–397. doi:10.1107/S0021889801002904.

[26] P. Scherrer, Estimation of the size and internal structure of colloidal particles by means of Röntgen rays, Göttinger Nachrichten Math. Phys. 2 (1918) 98–100.

[27] G.L. Chiarello, M.H. Aguirre, E. Selli, Hydrogen production by photocatalytic steam reforming of methanol on noble metal-modified TiO_2, J. Catal. 273 (2010) 182–190. doi:10.1016/j.jcat.2010.05.012.

[28] M. Janczarek, E. Kowalska, On the Origin of Enhanced Photocatalytic Activity of Copper-Modified Titania in the Oxidative Reaction Systems, Catalysts. 7 (2017) 317. doi:10.3390/catal7110317.